Flow (2024), **4** E25
doi:10.1017/flo.2024.27

FLOW CAMBRIDGE UNIVERSITY PRESS

RESEARCH ARTICLE

An extension of Thwaites' method for turbulent boundary layers

Rahul Agrawal[1,*], Sanjeeb T. Bose[2,3], Kevin P. Griffin[4] and Parviz Moin[1]

[1]Center for Turbulence Research, Stanford University, Stanford, CA 94305, USA
[2]Cadence Design Systems, San Jose, CA 95134, USA
[3]Institute for Computational and Mathematical Engineering, Stanford University, Stanford, CA 94305, USA
[4]National Renewable Energy Laboratory, Golden, CO 80401, USA
*Corresponding author. E-mail: rahul29@stanford.edu

Received: 21 June 2024; **Revised:** 5 September 2024; **Accepted:** 17 September 2024

Keywords: Integral method; turbulent boundary layers; flow separation

Abstract

Thwaites (*Aeronaut. Q.*, vol. 1, 1949, pp. 245–280) developed an approximate method for determining the evolution of laminar boundary layers. The approximation follows from an assumption that the growth of a laminar boundary layer in the presence of pressure gradients could be parameterized solely as a function of the Holstein–Bohlen flow parameter, thus reducing the von Kármán momentum integral to a first-order ordinary differential equation. This method is useful for the analysis of laminar flows, and in computational potential flow solvers to account for the viscous effects. In this work, an approximate method for determining the momentum thickness of a two-dimensional, turbulent boundary layer is proposed following Thwaites' work. It is shown that the method provides good estimates of the momentum thickness for multiple boundary layers, including both favourable and adverse pressure gradient effects, up to the point of separation. In the limit of high Reynolds numbers, it is possible to derive a criterion for the onset of separation from the proposed model, which is shown to be in agreement with prior empirical observations (Alber, *9th Aerospace Sciences Meeting, 1971*). The sensitivity of the separation location with respect to upstream perturbations is also analysed through this model for the NASA/Boeing speed bump and the transonic Bachalo–Johnson bump.

Impact Statement

The Thwaites' method (1949) for predicting the momentum thickness of non-equilibrium laminar boundary layers is extended to the turbulent regime. Validation is performed with high-fidelity numerical simulations and high Reynolds number experimental data. The proposed model agrees favourably with the reference datasets and provides a separation criterion at high Reynolds numbers; these can be useful in initial design processes and in determining the influence of flow history effects in canonical flow configurations.

1. Introduction

Often in the early stages of the engineering design processes, viscous effects are estimated using boundary layer integral methods. Common elements in many such engineering flows are that boundary layers are turbulent and subjected to strong pressure gradients – both favourable and adverse.

Clauser (1954, 1956) studied turbulent boundary layers and defined a parameter, β that quantifies the relative strength of the pressure gradient in relation to the skin friction across the boundary layer,

$$\beta = \frac{\delta^*}{\rho u_\tau^2}\frac{\mathrm{d}P}{\mathrm{d}s}, \tag{1.1}$$

where δ^* is the displacement thickness, $\mathrm{d}P/\mathrm{d}s$ is the pressure gradient and u_τ is the friction velocity. This parameter has since been used in analysing equilibrium and non-equilibrium boundary layers. In the presence of strong and/or prolonged favourable pressure gradients, the flow may relaminarize (Sreenivasan 1982). On the other hand, in the presence of adverse pressure gradients, it is possible for the flow to eventually separate (Simpson 1981, 1983), often associated with periods of rapid growth of the boundary layer. An adverse pressure gradient significantly energizes the outer flow (Knopp *et al.* (2021) showed that the viscously scaled turbulent stresses increase in the outer region of the boundary layer), and increases the momentum deficit compared with a zero pressure gradient boundary layer.

In the limit of thin boundary layers, the growth rate of the momentum thickness is related to the pressure gradient as follows (via the von Kármán momentum integral, see White (2008) for more details):

$$\frac{\mathrm{d}\theta}{\mathrm{d}s} = \frac{C_f}{2} + (2+H)\frac{\theta}{\rho U_e^2}\frac{\mathrm{d}P_e}{\mathrm{d}s}, \tag{1.2}$$

where θ is the momentum thickness, and C_f is the skin-friction along the streamwise coordinate. Here H is the shape factor which is the ratio of the displacement and the momentum thickness lengths of the boundary layer. However, this equation, in itself, is not particularly useful as a predictive tool and requires the knowledge of the skin friction and shape function distributions, which may be unknown *a priori*.

For laminar boundary layers, Thwaites (1949), and later Curle & Skan (1957), and Dey & Narasimha (1990) fitted data for various flows, including those with pressure gradients and flows undergoing separation, to derive an approximate expression for the growth of the momentum thickness for a given inviscid (free stream) velocity distribution. This analysis, coupled with the Falkner & Skan (1931) analysis in the viscous layer, provides a complete description of the mean velocity profile of the corresponding laminar flow. However, a similar analysis for turbulent boundary layers is more complex. Head (1958) proposed an integral momentum equation-based approach for turbulent boundary layers using the Ludwieg & Tillmann (1950) correlations. Weber (1978) developed a similar method (Coles & Hirst 1968; Kline *et al.* 1969). Das (1987), Das & White (1986) and Kalkhoran & Wilson (1986) developed integral approaches for measuring skin friction in turbulent boundary layers. A drawback of the approaches of Das (1987) and Das & White (1986) includes the use of multiple empirical correlations while also not accounting for history effects. Kalkhoran & Wilson (1986) made equilibrium assumptions for the boundary layer wake profile and the pressure gradient even for non-equilibrium boundary layers. A comprehensive review of these approaches can be found in Das *et al.* (2004).

It is apparent from the aforementioned efforts that further developments in the understanding of the growth of turbulent boundary layers are needed to improve potential flow solvers to account for pressure gradient effects. In this work, we have developed a model for predicting the momentum thickness of a turbulent boundary layer by extending Thwaites' method using a set of high-fidelity simulation data. The rest of this article is organized as follows. Section 2 describes the original Thwaites method for laminar flows. Section 3 summarizes some existing methods for predicting the momentum thickness of turbulent boundary layers. Section 4 provides the proposed extension to turbulent flows. Section 5 describes the simulation database used in this study. Section 6 describes the model coefficients and their validation in several flows. Section 7 discusses an application of the model in terms of the sensitivity of the separation parameter to flow perturbations. Some limitations of the proposed model are discussed in § 8. Concluding remarks are offered in § 9.

https://doi.org/10.1017/flo.2024.27 Published online by Cambridge University Press

2. Thwaites method for laminar boundary layers

In this section, a brief summary of the method of Thwaites (1949) for approximating the momentum thickness of laminar boundary layers is provided. For thin boundary layers in an incompressible flow, the von Kármán integral equation (White 2008) is written as

$$\frac{\mathrm{d}\theta}{\mathrm{d}s} + (2+H)\frac{\theta}{U_e}\frac{\mathrm{d}U_e}{\mathrm{d}s} = \frac{C_f}{2}, \tag{2.1}$$

where in the n–s coordinate system, s is the streamwise coordinate, and n is the wall-normal coordinate. Here δ^* and θ are the boundary layer's displacement and momentum thickness lengths, respectively, and $H = \delta^*/\theta$ is the shape factor. The following relations also hold under the thin boundary layer approximation:

$$\nu \left.\frac{\partial^2 U}{\partial n^2}\right|_{n=0} = \frac{1}{\rho}\frac{\mathrm{d}P_e}{\mathrm{d}s} = -U_e\frac{\mathrm{d}U_e}{\mathrm{d}s}, \tag{2.2}$$

where P_e and U_e are the values of the pressure and the streamwise velocity at the edge of the boundary layer, and $n = 0$ refers to the wall. This relation invokes $\mathrm{d}P/\mathrm{d}n \to 0$ within the boundary layer under the thin boundary layer approximation. Thus, the $\mathrm{d}P/\mathrm{d}s$ at the edge of the boundary layer ($\mathrm{d}P_e/\mathrm{d}s$) is considered to be approximately the same as that on the wall ($n = 0$). Using these relations, (2.1) is rearranged as

$$2Re_\theta\frac{\mathrm{d}\theta}{\mathrm{d}s} = 2((2+H)m + \chi) = L, \tag{2.3}$$

where m is the Holstein–Bohlen pressure gradient parameter, $m = (\theta^2/U_e)(\partial^2 U/\partial n^2)|_{n=0}$ and $\chi = (\theta/U_e)(\partial U/\partial n)|_{n=0}$. It should be noted that in deriving (2.3), the assumption of a laminar flow has not yet been invoked. For laminar boundary layers, however, Thwaites further postulated that $L = L(m)$, or that the effect of the pressure gradient primarily determines the growth rate of a laminar boundary layer. Specifically, the linear fit proposed in Thwaites' original work is

$$L \approx L(m)^{Thwaites} \approx 0.45 + 6m. \tag{2.4}$$

Rearranging the model fit, an approximate closed-form expression of the momentum thickness can be written as

$$\theta^2(s) \approx 0.45\frac{\nu}{U_e^6}\int_0^s U_e^5(r)\,\mathrm{d}r. \tag{2.5}$$

Further, Thwaites fitted experimental data to suggest that a laminar flow may separate when $m \approx 0.09$. Other similar empirical thresholds have been proposed by Stratford (1959) and by Curle & Skan (1957). More details can be found in Horton (1968). Curle & Skan (1957), and later Dey & Narasimha (1990) suggested slightly different model coefficients that resulted in a better agreement with the Blasius and Falkner–Skan type solutions.

3. Methods for turbulent flows

In this section, two commonly known methods for predicting the momentum thickness of a turbulent boundary layer in the presence of a pressure gradient are described.

3.1. Head's integral momentum equation

Similar to Thwaites' method for laminar boundary layers, Head (1958) and Head & Patel (1968) proposed an integral momentum equation-based approach for predicting the growth of the momentum

https://doi.org/10.1017/flo.2024.27 Published online by Cambridge University Press

thickness and the location of a separation point for turbulent boundary layers. The original work (Head 1958) was developed as follows. Using the correlation for the skin-friction (from Ludwieg & Tillmann (1950)) and an auxiliary relation between the shape factor (H) and the entrainment factor (H_1), a system of two differential equations governing the growth of the momentum thickness is given as

$$\frac{\mathrm{d}\theta}{\mathrm{d}s} + (2+H)\frac{\theta}{U_e}\frac{\mathrm{d}U_e}{\mathrm{d}s} = \frac{C_f}{2}, \tag{3.1}$$

$$C_f = 0.246(10^{-0.678H})Re_\theta^{-0.268}, \tag{3.2}$$

with the shape factor (H) and the entrainment factor (H_1) related as

$$\frac{1}{U_e}\frac{\mathrm{d}}{\mathrm{d}s}(U_e\theta H_1) = 0.0299(H_1 - 3.0)^{-0.6169}, \tag{3.3}$$

and $H_1 = 0.8234(H-1.1)^{-1.287}$ for $H \leq 1.6$, and $H_1 = 1.55(H-0.6778)^{-3.064} + 3.3$ otherwise. Head (1958) and the further developments in Head & Patel (1968) showed that the method can reasonably predict the growth of the momentum thickness for two-dimensional, non-equilibrium boundary layers. It is remarked that compared with Thwaites' method (which requires one empirical correlation), this approach requires additional correlations ((3.2)–(3.3) and $H_1 = f(H)$). For a comprehensive review, the reader is referred to Cebeci & Bradshaw (1977).

3.2. Drela's method

The method of Giles & Drela (1987), Drela & Giles (1987) and Drela (1989) has also been used to account for the viscous effects over airfoil flows. This formulation combines a potential flow panel method and an integral approach within the boundary layer. The viscous solution requires a correlation for the skin friction in terms of the shape factor to close the exact integral momentum equations. For an incompressible boundary layer, the invoked correlation from Swafford (1983) is given as

$$C_f = 0.3\,\mathrm{e}^{-1.33H}[\log_{10}(Re_\theta)]^{-1.74-0.31H} + 0.00011\left[\tanh\left(4 - \frac{H}{0.875}\right) - 1\right] \tag{3.4}$$

and a nonlinear system is solved to determine H as follows. When $H < H_0$,

$$H = 1.505 + \frac{4}{Re_\theta} + \left(0.165 - \frac{1.6}{Re_\theta^{0.5}}\right)\frac{(H_0 - H)^{1.6}}{H}, \tag{3.5}$$

otherwise

$$H = 1.505 + \frac{4}{Re_\theta} + (H - H_0)^2\left[\frac{0.04}{H} + \frac{0.007\log(Re_\theta)}{(H - H_0 + 4/\log(Re_\theta))^2}\right], \tag{3.6}$$

where $H_0 = 4$ when $Re_\theta < 400$ or else $H_0 = 3 + 400/Re_\theta$.

Both these approaches differ significantly from Thwaites' method in that the terms of the integral momentum boundary layer equation relating to the shape factor, H, and skin friction coefficient, C_f, are explicitly modelled. The present method described below attempts to make a direct extension of the Thwaites' transformation, without explicitly invoking a correlation for C_f, Reynolds number, Re_θ, and the shape factor, H.

4. Extension of Thwaites method to turbulent flows

In this section, we develop the proposed extension of Thwaites method for high Reynolds number turbulent boundary layers.

https://doi.org/10.1017/flo.2024.27 Published online by Cambridge University Press

Consider a zero pressure gradient turbulent boundary layer at a high Reynolds number. The growth rate of the momentum thickness of a turbulent boundary layer is higher than that of an equivalent Blasius laminar boundary layer ($\theta/s \sim Re_s^{-1/2}$). Reconciling this fact with the fact that (2.3) still holds for turbulent flows, the approximation made by Thwaites in (2.4), $L = L(m)$ must not hold for turbulent boundary layers. Since a boundary layer at a higher Reynolds number is less sensitive to the effects of pressure gradients (Vinuesa *et al.* 2018), the growth rate cannot depend only on the pressure gradient (as it did in the laminar case). Therefore, it is proposed that the growth rate of the momentum thickness may also depend directly on the Reynolds number. Equation (2.3) can be re-expressed as

$$2\frac{\mathrm{d}\theta}{\mathrm{d}s} = 2\frac{(2+H)m}{Re_\theta} + \frac{2\chi}{Re_\theta}. \tag{4.1}$$

The right-hand side of (4.1) contains four non-dimensional groups, m/Re_θ, mH/Re_θ, χ/Re_θ and $1/Re_\theta$. Similar to Thwaites (1949), where the sum of the terms is modelled purely as a function of m, we model the aggregate sum in terms of m and Re_θ. An explicit dependence of Re_θ is introduced to account for the scale separation between the inner and outer scales in a turbulent boundary layer. We admit a Taylor series approximation at high Reynolds number in terms of m/Re_θ and $1/Re_\theta$ for $m/Re_\theta \ll 1$ and $1/Re_\theta \ll 1$ to approximate the right-hand side of (4.1):

$$2\frac{\mathrm{d}\theta}{\mathrm{d}s} \approx C_{Re,\infty} + C_m\frac{m}{Re_\theta} + C_c\frac{1}{Re_\theta} + C_{m,2}\left(\frac{m}{Re_\theta}\right)^2 + C_{c,2}\left(\frac{1}{Re_\theta}\right)^2 + C_{m,c}\left(\frac{1}{Re_\theta}\right)\left(\frac{m}{Re_\theta}\right) + \cdots, \tag{4.2}$$

where $C_{(\cdot)}$ are the coefficients of the Taylor expansion. Implicitly, this approach assumes that $mH/Re_\theta, \chi/Re_\theta$ can be parameterized in terms of the remaining two groups ($1/Re_\theta$ and m/Re_θ). This modelling choice is made by observing that the shape factor $H \sim 1$–2 maintains a relatively constant order of magnitude in attached turbulent boundary layers. Secondly, the term, $\chi/Re_\theta = C_f/2$ has been subsumed into the other terms (formed from $1/Re_\theta$ and m/Re_θ) in the same spirit as the original work of Thwaites (1949). Further, $m/Re_\theta = (\theta/\rho U_e^2)(\mathrm{d}P_e/\mathrm{d}s)$ is a ratio of the viscous deficit length scale within the boundary layer to the momentum transport in the inviscid flow region; thus m/Re_θ may generally be expected to be small, at least, for attached boundary layers. This expectation is validated with additional data in the supplementary material available at https://doi.org/10.1017/flo.2024.27 accompanying this article. In the limit of $m/Re_\theta, 1/Re_\theta \ll 1$, the linear truncation is given by

$$2\frac{\mathrm{d}\theta}{\mathrm{d}s} \approx C_{Re,\infty} + C_m\frac{m}{Re_\theta} + C_c\frac{1}{Re_\theta}. \tag{4.3}$$

The error in the truncation of this Taylor series can be estimated as follows. For 'large' values of m/Re_θ, $1/Re_\theta$, still satisfying m/Re_θ, $1/Re_\theta \leq 1$ (this is not unreasonable since $m/Re_\theta = (\theta/\rho U_e^2)(\mathrm{d}P_e/\mathrm{d}s) \geq 1$ would imply that the viscous momentum deficit length scale within the boundary layer is larger than the inviscid flow's length scale; also, a boundary layer satisfying $Re_\theta \leq 1$ is likely non-turbulent), the truncation error in this model is governed by the quadratic terms, $(m/Re_\theta)^2$, $1/Re_\theta^2$, m/Re_θ^2. As will be shown in this article, the truncated model predicts θ with reasonable accuracy for Re_θ as low as ≈150. Assuming $Re_\theta \sim 150$, and $m/Re_\theta \sim 0.1$ (this estimate is an order of magnitude larger than the highest realized values of m/Re_θ in the database in this work, see the accompanying supplementary material) are acceptable lower limits of the validity of the proposed truncation, then the truncation error in the model is dominated by $\mathcal{E}(\mathrm{d}\theta/\mathrm{d}s) \sim (m/Re_\theta)^2 \sim 0.01 * C_{trunc}$ where C_{trunc} is some prefactor. This error may become comparable to the predicted value of $\mathrm{d}\theta/\mathrm{d}s$, governed by $m/Re_\theta \sim 0.1$. Thus, the proposed Taylor series truncation may be expected to perform poorly at low Reynolds number boundary layers under strong pressure gradients ($Re_\theta \leq O(100)$, $m/Re_\theta \geq O(0.1)$).

At higher Reynolds numbers, however, this model can be thought to be based on the assumptions that the growth of the boundary layer and the effect of the pressure gradient decreases with the Reynolds number. An interpretation of the linear model is that the effect of the pressure gradient and the Reynolds

https://doi.org/10.1017/flo.2024.27 Published online by Cambridge University Press

number are only weakly coupled. Rewriting (4.3) in terms of the definition of L in (2.3), the model form for L can be written as

$$L = L(m, Re_\theta) \approx C_c + C_m m + C_{Re,\infty} Re_\theta. \tag{4.4}$$

With this approximation, the growth rate of the momentum thickness is

$$\frac{\mathrm{d}}{\mathrm{d}s}(U_e^{C_m}\theta^2) \approx \nu C_c U_e^{C_m-1} + C_{Re,\infty} U_e^{C_m}\theta. \tag{4.5}$$

This ordinary differential equation can be integrated numerically along the streamwise direction if the inflow and the free stream conditions are known. The numerical values of C_c, C_m, $C_{Re,\infty}$ will be determined in § 6.

5. Database of pressure gradient flows

It has been well established that in the presence of strong pressure gradients, the upstream flow history affects the downstream development of the flow (Nickels 2004; Bobke *et al.* 2017; Vinuesa *et al.* 2017; Devenport & Lowe 2022). A comprehensive database of turbulent boundary layers is used in this work to account for many of these effects. Relevant details of the datasets are given below. Further, table 1 summarizes the range of the Reynolds number and the Clauser parameter for the boundary layers considered.

(i) Zero Pressure Gradient: Eitel-Amor *et al.* (2014) performed wall-resolved large-eddy simulations (LES) of a spatially developing zero pressure gradient boundary layer up to $Re_\theta = 8300$.

(ii) Adverse Pressure Gradient: Bobke *et al.* (2017) performed wall-resolved LES of five different boundary layers at varying Reynolds numbers and strength of pressure gradients. Two of these five boundary layers were maintained at nearly constant Clauser parameters, $\beta = 1$ and 2 while the other three boundary layers followed a power law for the streamwise velocity at the edge of the boundary layer, $U_e \sim (x - x_0)^q$ with $q = -0.13$, -0.16 and -0.18.

(iii) Airfoils: Vinuesa *et al.* (2018) and Tanarro *et al.* (2020) simulated the flow over two different NACA (National Advisory Committee for Aeronautics) airfoils, namely NACA 4412 and 0012, respectively, at varying chord-length-based Reynolds number and angles of attack. We consider three particular cases, NACA 0012 airfoil at $Re_c = 0.4 \times 10^6$, $\alpha = 0.0°$, and NACA 4412 airfoil at $Re_c = 0.1 \times 10^6$, 1×10^6, $\alpha = 5.0°$.

(iv) Smooth Body Separation: The problem of predicting smooth body separation in computational fluid dynamics has remained a challenge. Uzun & Malik (2022) performed a quasi-DNS of the flow over a smooth Gaussian bump as it experienced both a favourable pressure gradient, followed by an adverse pressure gradient, and thereafter a turbulent separation. These results were in agreement with the experiments of Williams *et al.* (2020).

(v) Shock Induced Separation: In external aerodynamic applications, weak compressibility effects affect the flow pattern due to the shock-formation, and the consequent flow separation at high Mach numbers. Uzun & Malik (2019) performed high-fidelity simulations of the experiments of Bachalo & Johnson (1986) that studied the flow over a hump on a cylinder experiencing shock and adverse pressure gradient induced flow separation.

The undetermined model coefficients, C_c, C_m and $C_{Re,\infty}$, are obtained from fitting the simulation data from the zero pressure gradient and adverse pressure gradients of Eitel-Amor *et al.* (2014) and Bobke *et al.* (2017), respectively. The remainder of the simulation database is used to assess the generality of the proposed model and fits. Overall, this dataset covers a Re_θ range of two decades ($150 \leq Re_\theta \leq 16\,000$). This range is comparable to the Reynolds numbers reported on the attached region of the flow over a transonic common research model aircraft at cruise configuration in Goc *et al.* (2023) from the leading edge up to 70% of the wing chord. It is worth mentioning that the Re_θ range from the chosen direct

https://doi.org/10.1017/flo.2024.27 Published online by Cambridge University Press

Table 1. *The variation in friction, momentum thickness-based Reynolds numbers and Clauser parameters in the datasets considered in this work. For the flows that experience separation (FPG/APG SBSE and FPG/APG BJ), only preseparation data is considered. Since both favourable and adverse pressure gradient boundary layers are included, the Clauser parameter varies from a negative to a positive value.*

Dataset	Range of Re_τ	Range of Re_θ	Range of β
ZPG (Eitel-Amor, Örlü & Schlatter 2014)	[180,2500]	[350,7900]	= 0
APG (Bobke *et al.* 2017)	[200,1000]	[500,4200]	[1, 5]
Airfoils (Vinuesa *et al.* 2018; Tanarro, Vinuesa & Schlatter 2020)	[100,700]	[150,6900]	[1, 85]
FPG/APG SBSE (Uzun & Malik 2022)	[400,1200]	[1000,4600]	[-2, 15]
FPG/APG BJ (Uzun & Malik 2019)	[1500,4000]	[3000,16 000]	[-6, 6]

numerical simulations (DNS) or wall-resolved LES in the present dataset is similar to that of mean two-dimensional, boundary layer experiments considered in Cebeci, Mosinskis & Smith (1970) to determine the efficacy of Head's method (Head 1958) in § 3. The proposed model is validated for three additional cases from experimental measurements at higher Reynolds numbers (Skare & Krogstad 1994; Nagib, Christophorou & Monkewitz 2006; Vila *et al.* 2020) in Appendix A.

6. Model coefficients and validation

6.1. Fitting model coefficients

The model coefficients C_c, C_m and $C_{Re,\infty}$ are determined in two stages. Since $m = (\theta^2/U_e)(\partial^2 U/\partial n^2)|_{n=0} = 0$ for a zero pressure gradient boundary layer, the coefficients C_c and $C_{Re,\infty}$ are determined from the data of Eitel-Amor *et al.* (2014) alone using a least-squares fit (with bisquare weights). Here C_m is finally found using the wall-resolved LES data of boundary layers under slightly dissimilar pressure gradients (Bobke *et al.* 2017). The numerical values of the coefficients obtained are $C_c = 1.45$, $C_{Re,\infty} = 0.0024$ and $C_m = 7.23$ with the corresponding 95 % confidence intervals $C_c \in [1.43, 1.47]$, $C_{Re,\infty} \in [0.0023, 0.0025]$ and $C_m \in [7.20, 7.25]$, respectively.

Using (4.5), the variation in θ versus s is compared with the values obtained from mean velocity profiles using the method of Griffin, Fu & Moin (2021) (in this article, the integral for θ was terminated at the edge of the boundary layer, thus ignoring any inviscid flow contribution to the momentum thickness). Figures 1 and 2 show the model fit for the zero-pressure gradient boundary layer and the adverse pressure gradient boundary layers, respectively. The growth rate of θ is reasonably predicted with minor discrepancies near the domain outlet. These discrepancies may be attributed to the presence of a fringe region at the outflow in the reference simulations at $x/\delta_0^* \approx 2500$ (in this article, the symbol δ_0^* refers to the displacement thickness at the flow inlet). The corresponding Re_θ are presented in the right-hand abscissa of figure 1, and in figure 2(*b*). These highlight that the fitted data predominantly lies within an $Re_\theta \sim O(10^3)$ range. These fits will be validated in both lower and higher Re_θ regimes in the subsequent sections.

Although not shown, the shape factor for these boundary layers was found to vary significantly across the cases, and not follow a simple linear fit in (m, Re_θ) space. Laminar potential flow solvers iteratively solve for θ from Thwaites method and find δ^* from the $H = H(m)$ relationship to determine the 'effective body shape' due to flow acceleration. For turbulent flows, since $H = H(m)$ is non-universal, this approach is not workable. The accompanying supplementary material provides an alternate approach for finding the growth rate of the displacement thickness using boundary layer edge variables.

https://doi.org/10.1017/flo.2024.27 Published online by Cambridge University Press

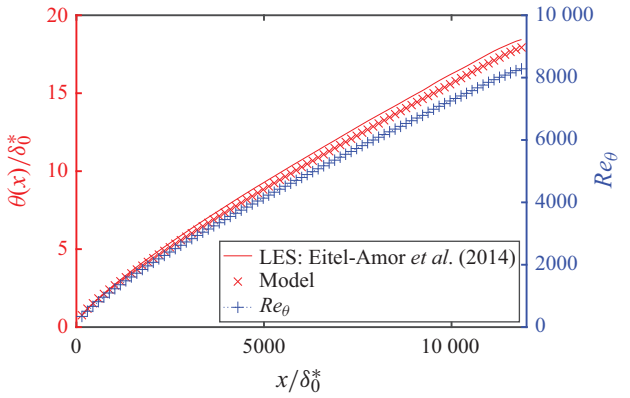

Figure 1. *Fit of θ versus the streamwise distance x/δ_0^* for the zero pressure gradient boundary layer in Eitel-Amor et al. (2014). The vertical axis on the right-hand side of the panel presents the true LES Re_θ as a function of the streamwise coordinate.*

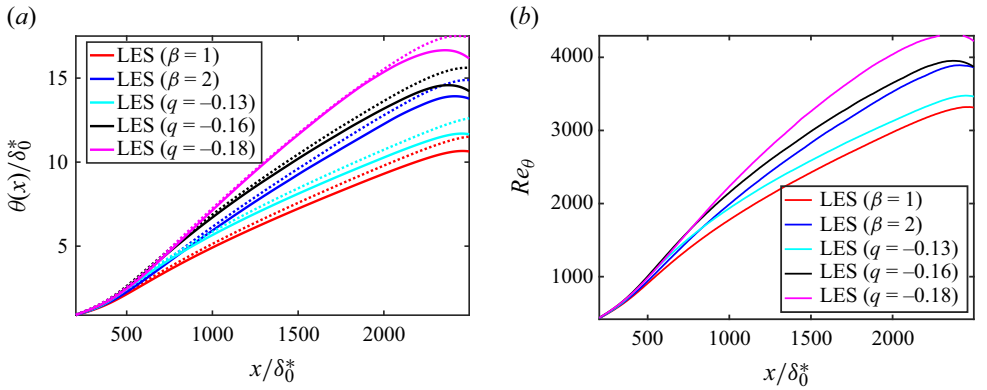

Figure 2. *(a) Fit of θ versus the streamwise distance x/δ_0^* for the adverse pressure gradient boundary layers in Bobke et al. (2017). The solid lines denote the values obtained from the reference simulations, and the dotted lines refer to the model fit. Panel (b) presents the true (LES) corresponding Re_θ at the streamwise stations.*

6.2. Testing on APG wing data

This section evaluates the model for two airfoil flows at low angles of attack published in Vinuesa *et al.* (2018) and Tanarro *et al.* (2020). Two NACA airfoils at different chord-based Reynolds numbers (Re_c) and angles of attack (α) are considered: a NACA 0012 airfoil at $Re_c = 0.4 \times 10^6$, $\alpha = 0°$ and NACA 4412 airfoil at $Re_c = 0.1 \times 10^6$ and $Re_c = 1.0 \times 10^6$, $\alpha = 5°$. Note that the dataset available for these airfoils only provides detailed statistics beyond $x/c = 15$ % as the flow is tripped at $x/c = 0.1$.

For these cases, the pressure gradient distributions are quite different, as quantified by the Clauser parameter in figure 3(*a*). Near the trailing edge, the pressure gradient for NACA 4412 airfoils varies quite significantly, and its effect is much stronger than that of the wall shear stress (β eventually reaches up to ≈ 85 at $x/c \approx 0.99$), suggesting a highly non-equilibrium, or a nearly separated flow. In figure 3(*b*), at the trailing edge of the NACA 4412 airfoil case, the momentum thickness (θ/θ_0, where θ_0 in this article refers to an upstream momentum thickness; for the wing data, this reference point is at $x/c = 0.15$) is underpredicted from the proposed fit suggesting a simple linear model is only partially capturing the history effects from the pressure gradients when the Clauser parameter, β, grows quickly and approaches

https://doi.org/10.1017/flo.2024.27 Published online by Cambridge University Press

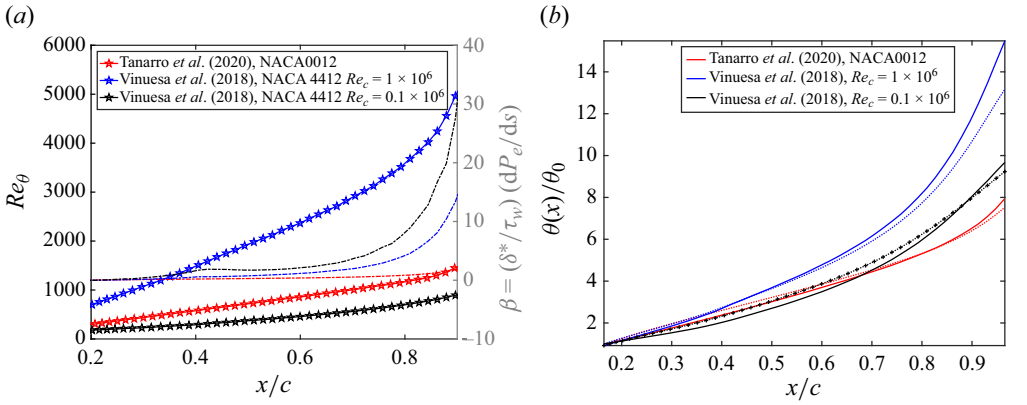

Figure 3. *(a) The LES predicted momentum thickness based Reynolds number, Re_θ, and the Clauser parameter, β, as a function of the streamwise distance, x/c. The starred lines correspond to the Re_θ, and the dashed lines with no symbols correspond to β. (b) The fit of θ/θ_0 versus x/c for a NACA 0012 airfoil at $Re_c = 0.4 \times 10^6$, angle of attack $\alpha = 0°$ (LES of Tanarro et al. (2020)) and for a NACA 4412 airfoil at $Re_c = 0.1,\ 1 \times 10^6$, angle of attack $\alpha = 5°$ (LES of Vinuesa et al. (2018)), respectively.*

very large values, a marker of intermittently separating flows. The increased Reynolds number was found to be responsible for the lowered β between the two NACA 4412 airfoils (Vinuesa *et al.* 2017).

6.3. Testing on SBSE and BJ data

Smooth body separation refers to the flow condition where neither the separation nor reattachment points of a separation bubble are geometrically imposed. As a result, the flow development history (i.e. the influence of pressure gradients and/or compressibility) affects the tendency of the flow to separate. Uzun & Malik (2022) recently performed a quasi-DNS of flow over a spanwise-periodic Gaussian bump in which the flow separates on the leeward side of the bump due to the mild, adverse pressure gradient. Similarly, the wall-resolved LES of Uzun & Malik (2019) is an example of shock-induced separation in a transonic flow over a bump. Figure 4 shows a schematic of the bump geometries and the case set-up for both flows. For both flows, an incoming zero-pressure gradient turbulent boundary layer experiences a favourable pressure gradient, which accelerates the flow before eventually experiencing an adverse pressure gradient that leads to flow separation. Although not shown, the variation in the Clauser parameter, Reynolds numbers along the streamwise direction until the point of separation ($x/L \sim 0.1$ for the SBSE and $x/c \sim 0.65$ for the BJ) are significantly different.

As seen in figure 5, the proposed model predicts the momentum thickness for both these flows reasonably up to the point of separation (for the transonic flow, Uzun & Malik (2019) performed their simulations at $Ma = 0.875$ at which the location of the shock, and the separation nearly coincide (Bachalo & Johnson 1986)). The Re_θ (right-hand abscissa in figure 5*a*,*b*) for both these flows does not monotonically increase as the flow experiences a favourable pressure gradient (not seen in 'training' cases). Further, the Re_θ on the transonic bump reaches values $Re_\theta \sim O(10^4)$, larger than those in the training sets. We remark that inside the separation bubble, the thin boundary layer approximation utilized breaks down, and as such, this model is not expected to perform well.

It is also highlighted that the proposed model was derived for incompressible flows and neglected any variations in density in the flow across the boundary layer. The transonic flow in Uzun & Malik (2019) was locally supersonic in the favourable pressure gradient region exhibiting a density gradient across the boundary layer; the ratio of the mean density in the free stream and the wall ≈ 2, and a normalized density gradient, $\boldsymbol{\nabla}\rho \gg 1$ (the reader is referred to figure 1 in Uzun & Malik (2019) for more details). A more complete analysis of compressible turbulent boundary layers suggests that the ratio of

https://doi.org/10.1017/flo.2024.27 Published online by Cambridge University Press

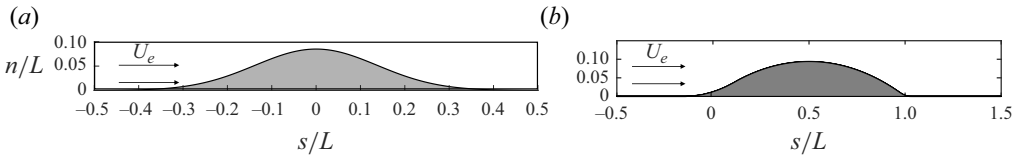

Figure 4. *A schematic of the surface geometry over which the turbulent flow separates in the (a) subsonic Boeing speed bump case of Uzun & Malik (2022) and (b) transonic flow case of Uzun & Malik (2019). Here L and c are the characteristic lengths for the two cases, respectively; U_e is the free stream flow velocity, and the arrows next to it point along the positive streamwise direction.*

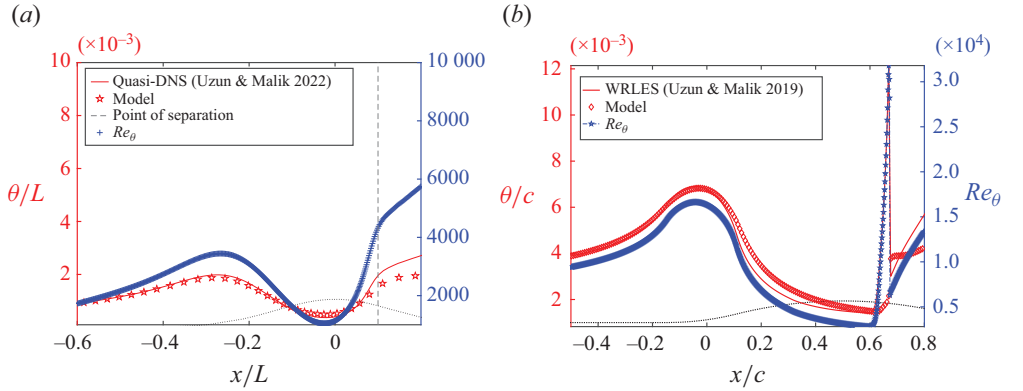

Figure 5. *Fit of θ versus the streamwise distance x non-dimensionalized by the respective bump widths. Panel (a) presents the model fit and the true Re_θ for the Boeing speed bump in Uzun & Malik (2022), and (b) presents the model fit and the true Re_θ for the wall-resolved LES (WRLES) of the transonic Bachalo–Johnson bump in Uzun & Malik (2019). The solid vertical lines denote the separation point as obtained from the reference data. Note that $x/L = 0$ is the position of the apex of the Boeing speed bump, whereas $x/c = 0.5$ is the position of the apex of the transonic bump.*

the free stream to wall temperature (or equivalently densities) should appear as an additional factor in the Taylor series expansion, which may account for some of the observed differences between the reference data and the proposed model. A comparison between the proposed model and the existing methods (in § 3) for flow over the Boeing speed bump geometry is presented in Appendix B.

The proposed model can be used to help predict the conditions under which the separation of the boundary layer is imminent. To date, there have been numerous attempts to characterize this point of separation empirically. Alber (1971) proposed that separation is imminent when $(\theta/\rho_e U_e^2)(\mathrm{d}P_e/\mathrm{d}s) > 0.004$. The exact value of the threshold was determined empirically for some weakly compressible flows and is relatively robust in the presence of weak shocks (Alber *et al.* 1973; Adair 1987). As seen in figure 6 the value of $(\theta/\rho_e U_e^2)(\mathrm{d}P_e/\mathrm{d}s)$ is approximately 0.004 at the location of separation for both the flow over the Boeing speed bump and the flow in the Bachalo–Johnson experiments. For laminar flows, Thwaites also proposed a fit between the shape factor, H, and the Holstein–Bohlen parameter, m, that allowed computation of the skin friction using the local value of m. Using this analysis, the separation boundary for a laminar flow was suggested to be $m = 0.09$. Although not shown, we have observed that the two flows considered in this work exhibited separation for different values of m, and thus m alone cannot be used to predict flow separation in turbulent flows.

Alternatively, it is possible to estimate the value of the Alber separation parameter by using the proposed model. For a locally constant and finite pressure gradient, the proposed model suggests that $\mathrm{d}\theta/\mathrm{d}s$ is a linear function of $(\theta/\rho_e U_e^2)(\mathrm{d}P_e/\mathrm{d}s)$ (the reader is referred to (4.3) and the fact that $m/Re_\theta = (\theta/\rho_e U_e^2)(\mathrm{d}P_e/\mathrm{d}s)$). Using the von Kármán integral equation, this equation can be further

https://doi.org/10.1017/flo.2024.27 Published online by Cambridge University Press

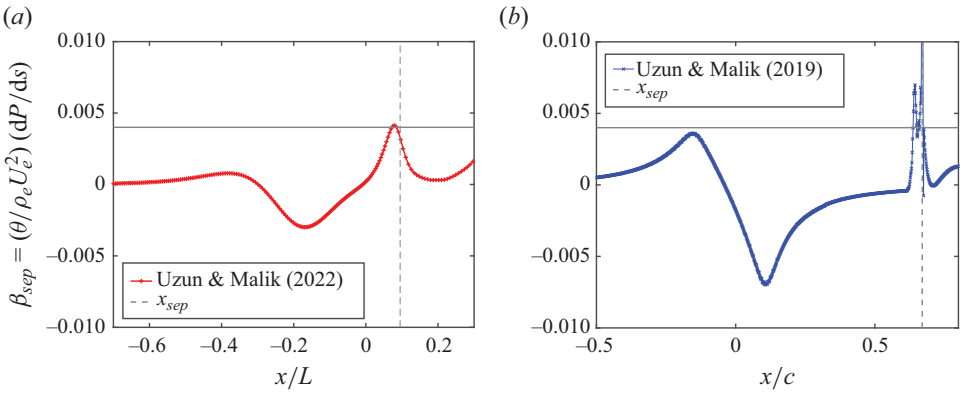

Figure 6. *The variation in the non-dimensional group* $(\theta/\rho_e U_e^2)(\mathrm{d}P/\mathrm{d}s)$ *along the streamwise direction for the (a) Boeing speed bump in Uzun & Malik (2022) and the (b) transonic Bachalo–Johnson bump in Uzun & Malik (2019). The dashed vertical lines denote the separation point as obtained from the reference data. Note that* $x/L = 0$ *is the position of the apex of the Boeing speed bump, whereas* $x/c = 0.5$ *is the position of the apex of the transonic bump.*

simplified as

$$\frac{C_f}{2} \approx \frac{C_c}{2}\frac{\nu}{U_e\theta} + \frac{C_{Re,\infty}}{2} + \left(\frac{C_m}{2} - (2+H)\right)\frac{\theta}{\rho U_e^2}\frac{\mathrm{d}P_e}{\mathrm{d}s}. \tag{6.1}$$

In the limit of an asymptotically large Reynolds number ($Re_\theta \to \infty$) flow nearing separation, and estimating $H \approx 2.0$, yields that the separation is imminent when

$$\frac{\theta}{\rho U_e^2}\frac{\mathrm{d}P_e}{\mathrm{d}s} \approx \frac{-C_{Re,\infty}}{2\left(\dfrac{C_m}{2} - (2+H)\right)} \approx 0.003, \tag{6.2}$$

which is similar to the empirical threshold proposed by Alber (1971). It is noted that although Re_θ does not strictly tend to an infinite value at the point of separation in most flows: for $Re_\theta \gg 600$ at the separation point, the first term on the right-hand side of (6.1) becomes much smaller than the second term ($C_{Re,\infty}/2$), thus removing any explicit dependence of the value of Alber's parameter on Re_θ. It is highlighted that the estimate of $H \approx 2$ is only made to compare the orders of magnitude of the threshold value of $\theta/(\rho_e U_e^2)\,\mathrm{d}P_e/\mathrm{d}s$ for flow separation between the proposed model and that of Alber (1971). For instance, if a value of $H = 2.5$ is used, the threshold value (based on the present values of C_m, $C_{Re,\infty}$) of $\theta/(\rho_e U_e^2)\,\mathrm{d}P_e/\mathrm{d}s$ for flow separation $\approx$0.0014. Using this threshold value, the error (relative to the true value) in the predicted point of separation is $\Delta x/L \approx 0.06$ (on the Boeing speed bump) and $\Delta x/c \approx 0.04$ (on the Bachalo–Johnson bump), respectively. Similarly, the error incurred upon using a threshold value of 0.003 (in (6.2)) is $\Delta x/L \approx 0.03$ and $\Delta x/c \approx 0.03$ for the two bump flows, respectively. In this respect, the values of $H \approx 2$ or $H \approx 2.5$ are deemed to lead to the same order of error in determining the separation point.

Equation (6.1) also describes a nonlinear separation and reattachment criterion (in a space spanned by $1/Re_\theta$, H and $(\delta^*/U_e^2)(\mathrm{d}P_e/\rho\,\mathrm{d}s)$) for turbulent flows over smooth surfaces for a range of Reynolds numbers as

$$\frac{C_c}{2}\frac{\nu}{U_e\theta} + \left(\frac{C_m}{2} - (2+H)\right)\frac{\theta}{\rho U_e^2}\frac{\mathrm{d}P_e}{\mathrm{d}s} = -\frac{C_{Re,\infty}}{2}. \tag{6.3}$$

https://doi.org/10.1017/flo.2024.27 Published online by Cambridge University Press

7. Sensitivity analysis of separation using Alber's parameter

Accurate prediction of flows exhibiting separation from mild, adverse pressure gradients remains a pacing item for the development of closure models for both Reynolds-averaged Navier–Stokes and LES. In this section, we explore using the proposed model to quantify the impact of history effects in such flows. The following assumes that the point of separation is determined by Alber's parameter, as was motivated in the preceding section.

In wall-modelled LES, it is difficult to isolate the regions of deficiency of the near-wall model (for predicting the wall shear stress) in non-equilibrium flows, especially in flows undergoing smooth body separation. This is in part because it remains difficult to quantify the importance of history effects in the wall closure approximation. If we denote $J(\theta)_{sep} = -(\theta_{sep}/U_{e,sep})(\mathrm{d}U_{e,sep}/\mathrm{d}s)$ as the value of the Alber parameter at the point of separation, then the parameter $(m/J_{sep})(\mathrm{d}J_{sep}/\mathrm{d}m)$ is a relative measure of the sensitivity of flow separation parameter to upstream modelling deficiencies (quantified via m) since the perturbations in m (Δm or $\mathrm{d}m$ in the limit of $\Delta m \to 0$) can be thought of as arising due to the errors in the prediction of the wall stress. This sensitivity parameter can be re-expressed as

$$\frac{m}{J_{sep}}\frac{\mathrm{d}J_{sep}}{\mathrm{d}m} = \frac{m}{J_{sep}}\frac{\mathrm{d}J_{sep}}{\mathrm{d}J(\theta)} * \frac{\mathrm{d}J(\theta)}{\mathrm{d}m} = \frac{m}{J_{sep}}\frac{\mathrm{d}J_{sep}}{\mathrm{d}J(\theta)} * \frac{1}{2Re_\theta} = \frac{1}{2}\frac{\theta}{\theta_{sep}}\frac{\mathrm{d}\theta_{sep}}{\mathrm{d}\theta} = \frac{1}{2}\frac{\theta}{\theta_{sep}}\frac{1}{\dfrac{\mathrm{d}\theta}{\mathrm{d}\theta_{sep}}}. \tag{7.1}$$

Equation (7.1) quantifies the expected response in the value of J_{sep} for a given perturbation in m. Further, based on the last equality in (7.1), this sensitivity parameter can be completely determined by numerically perturbing the momentum thickness at the true point of separation (θ_{sep}) and integrating (4.3) backward (upstream). This provides the change in θ at all upstream locations due to a known perturbation in θ at the true separation point.

Figure 7 suggests that two different mechanisms are important for the two separating flows considered in this article. From figure 7(*a*), it is clear that for the Boeing speed bump, the sensitivity of Alber's parameter to a perturbation in m is non-local, or that a perturbation in m even far upstream, 30–40 δ_{sep}, will lead to a non-negligible change in J_{sep}. However, perturbations in the region after the apex (beyond the vertical dashed line, in the adverse pressure gradient region) are most important in that the imminently separating flow responds to those the most. The curve is increasing in the zero pressure gradient and the favourable pressure gradient region, which implies that the closer the perturbations are made to the separation point, the more responsive the tendency of the flow to separate. These results agree with Devenport & Lowe (2022) who suggest that the 'history effects' of pressure gradients in a turbulent boundary layer may extend up to 50δ (where δ is the local boundary layer thickness). However, in figure 7(*b*), for the transonic bump, the sensitivity is primarily localized in a smaller region after the apex (less than $5\delta_{sep}$), localized to the vicinity of the shock (marked by the dashed line). This suggests that for the Bachalo–Johnson bump flow, the prediction of separation is primarily governed by the shock and the adverse pressure gradient in its vicinity, or the upstream history or modelling errors are not that significant. These contrasting mechanisms in the two separating flows considered in this article provide evidence that flow separation can occur due to different flow development patterns.

8. Model limitations

Thus far, the proposed model has been shown to predict momentum thickness in several non-equilibrium turbulent boundary layers reasonably. However, we also highlight some potential limitations of the proposed model in specific flow regimes.

(i) Laminar or relaminarizing boundary layers. For laminar boundary layers, the original method of Thwaites (1949) is expected to produce more favourable results than the proposed method. This can be seen in that the proposed model's coefficients are larger than the equivalent coefficients in the original Thwaites' method. Further, for highly accelerated boundary layers with significant

https://doi.org/10.1017/flo.2024.27 Published online by Cambridge University Press

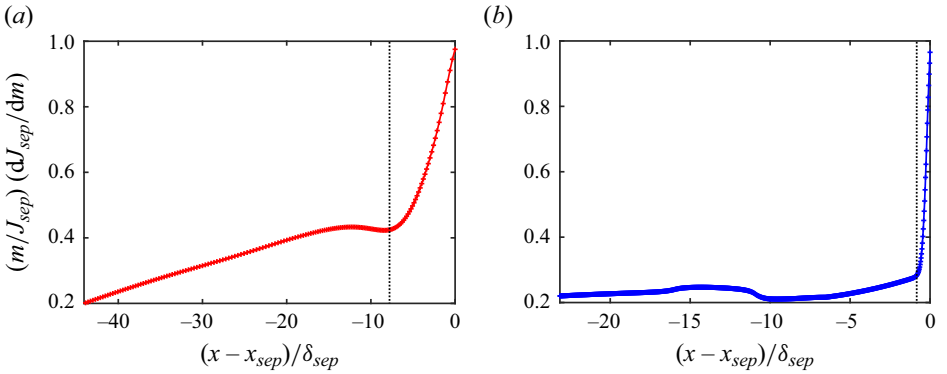

Figure 7. *The streamwise variation (non-dimensionalized by the boundary layer thickness at the point of separation) of the relative sensitivity of $J_{sep} = -(\theta/U_e)(\mathrm{d}U_e/\mathrm{d}s)$ evaluated at the point of separation to the upstream perturbations in the Holstein–Bohlen parameter, m, for (a) the Boeing speed bump and (b) the transonic Bachalo–Johnson bump. The dashed lines in panels (a) and (b) correspond to the location of the bump apex and the shock, respectively. Here, δ_{sep} is the thickness of the boundary layer at the true point of separation.*

relaminarization (Sreenivasan 1982), the proposed model is not expected to capture the reduced growth of the momentum thickness as the 'training dataset' only contains the purely turbulent flow regimes. For instance, although not shown, it was observed that for the strongly accelerated, relaminarizing boundary layer studied in Bourassa & Thomas (2009), the proposed model underpredicts the momentum thickness by approximately 60 % in the regions where the acceleration parameter, $K = \nu/U_e^2\,\mathrm{d}U_e/\mathrm{d}x \geq 2 \times 10^6$ (region of at least partial relaminarization).

(ii) Low Reynolds number turbulent boundary layers. As discussed in the model description, for $Re_\theta \leq 100$, the truncation error in the proposed model may become comparable to the model predictions. Thus, the model can be expected to fail for such low Reynolds numbers.

(iii) Large pressure gradients, and separated boundary layers. As also highlighted in § 4, for flows with very large pressure gradients, such that $m/Re_\theta \geq O(10^{-1})$, the proposed linear truncation (4.3) is not expected to determine the growth of the momentum thickness reasonably. Further, beyond the onset of a boundary layer separation, the proposed model has been shown to predict the momentum thickness incorrectly (see § 6.3). Such a flow regime is marked by a strong increase in the shape factor, with H, often reaching values higher than $H \gtrsim 2$. These regimes also coincide with sharp rises in the Clauser parameter ($\beta \gg 1$, such as in figure 3) as the shear stress drops to zero near a separation point.

(iv) High free stream turbulence. High free stream turbulence values can reduce the wake region of the boundary layer relative to a negligible free stream turbulence case (Thole & Bogard 1996), and increase the skin-friction (Hancock & Bradshaw 1983), thus also equivalently increasing $\mathrm{d}\theta/\mathrm{d}x$. Thus, in the presence of significant free stream turbulence, the present model may underpredict the growth of the momentum thickness. Future research may include the effects of free stream turbulence through an additional eddy-viscosity term such as in Volino (1998).

(v) Wall roughness. In boundary layers with wall roughness, there is an additional drag due to the pressure forces, which shift the mean velocity profile downward relative to a smooth wall (in viscous units). Generally, this form drag is represented in the doubly averaged form of the Navier–Stokes equations as a sink term (Talluru *et al.* 2016), which also modifies the von Kármán integral equation relative to (1.2). However, the present model ignores this added drag term and is thus expected to underpredict the growth of momentum thickness.

(vi) Compressible boundary layers. As observed on the fore side of the transonic Bachalo–Johnson bump, for a locally supersonic flow, the proposed model overpredicts the momentum thickness as the effect of the Mach number in the von Kármán integral equation has been ignored.

https://doi.org/10.1017/flo.2024.27 Published online by Cambridge University Press

(vii) Large Reynolds number limit. For $Re_\theta \to \infty$, in the absence of any pressure gradient, $\mathrm{d}\theta/\mathrm{d}s = C_f/2$ is smaller than the predicted $\mathrm{d}\theta/\mathrm{d}s = C_{Re,\infty}/2$ as C_f decreases with Re_θ (albeit weakly, see Nagib *et al.* (2006)). The fitted coefficient, $C_{Re/\infty}$ was based on a boundary layer at an $Re_\theta \sim O(10^4)$, and hence for a higher Reynolds number, for example, $Re_\theta \geq O(10^5)$ flow, the currently fitted model coefficients may be expected to overpredict the boundary layer growth.

(viii) Wall curvature. The effect of surface curvature on the accuracy of the proposed model has been briefly tested using the two bump flows (e.g. on the Boeing speed bump, $\delta/r_w \lessapprox 0.06$). For large curvatures, however, when $\delta/r_w \uparrow$ (r_w is the local radius of curvature of the wall) becomes larger, additional curvature correction terms would need to be included in the proposed model.

Future work may include further improvements to the proposed model to alleviate these model limitations.

9. Concluding remarks

This work presents an extension of the method of Thwaites for determining the momentum thickness for a turbulent boundary layer under the action of pressure gradients. In the limit of large Reynolds numbers, a linear model is hypothesized, such that the Reynolds number and pressure gradient dependence on the growth rate of the momentum thickness can be superposed. A fit for the model coefficients is found using recent high-fidelity simulation data for various boundary layers ranging from Reynolds number, $Re_\tau \approx [100, 4000]$ and Clauser parameter, $\beta, \approx [-6, 10]$. Generally, the model predicts the growth of the momentum thickness well for both favourable and adverse pressure gradient flows. The model is also used to derive a condition for imminent separation at high Reynolds numbers, which resulted in similar threshold values as previously work of Alber (1971). An application of the proposed method is demonstrated by estimating the importance of history effects on separation. Specifically, the importance of upstream history effects for the Boeing speed-bump flow is quantified. For a transonic bump flow, it is shown that only local perturbations just upstream of the shock location cause significant changes to the separation location.

Acknowledgements. We acknowledge helpful discussions with M. Whitmore at Stanford University.

Funding. This work was supported by NASA's Transformational Tools and Technologies project under grant no. #80NSSC20M0201 and by Boeing Research & Technology. K.P.G. is supported by the US Department of Energy Office of Energy Efficiency and Renewable Energy, the Wind Energy Technologies Office and the Exascale Computing Project (Grant17-SC-20SC). This work was authored in part by the National Renewable Energy Laboratory, operated by Alliance for Sustainable Energy, LLC, for the US Department of Energy (DOE) under contract no. DEAC3608GO28308. The views expressed in the article do not necessarily represent the views of the DOE or the US Government. The US Government retains and the publisher, by accepting the article for publication, acknowledges that the US Government retains a nonexclusive, paid-up, irrevocable, worldwide license to publish or reproduce the published form of this work or allow others to do so, for the US Government purposes.

Declaration of interests. The authors declare no conflict of interest.

Data availability statement. Raw data is accessible in the relevant publications referenced in this work.

Ethical standards. The research meets all ethical guidelines, including adherence to the legal requirements of the study country.

Author contributions. R.A., K.P.G. and S.T.B. created the research plan and analysis. R.A. and K.P.G. wrote the initial draft of the manuscript. S.T.B. and P.M. advised on the research and reviewed the manuscript.

Supplementary material. Supplementary material is available at https://doi.org/10.1017/flo.2024.27.

Appendix A. Performance of proposed model in boundary layers at high Reynolds number

Skare & Krogstad (1994) performed experiments of boundary layers at the verge of separation up to $Re_\theta = 5.4 \times 10^4$, by controlling the applied external pressure gradient. The shape factor, H, smoothly varied between $1.8 \leq H \leq 2$, and the Clauser parameter, β, varied between $12.2 \leq \beta \leq 20.4$. In the

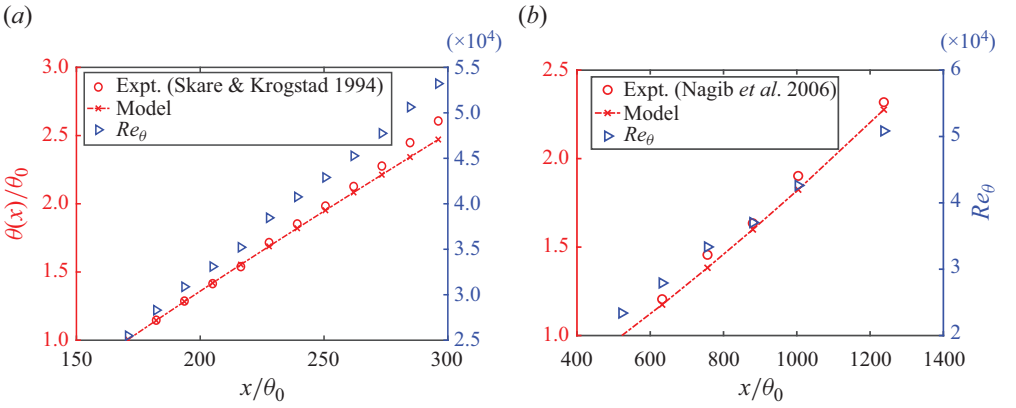

Figure 8. *The fit of θ/θ_0 versus the streamwise distance x/θ_0 for the experimental measurement stations reported in Skare & Krogstad (1994) for a high Reynolds number, under-equilibrium boundary layer on the verge of separation and in Nagib et al. (2006) for a canonical, weak adverse pressure gradient boundary layer. The left-hand and right-hand abscissas on these plots denote the prediction of θ and the true, experimental, value of Re_θ at the respective streamwise locations, respectively.*

latter half of this boundary layer, the free stream velocity followed an approximate power law along the streamwise distance, which is a condition for a boundary layer under finite pressure gradient to be 'under-equilibrium' (Castillo & George 2001; Castillo, Wang & George 2004). Similarly, Nagib *et al.* (2006) performed experiments up to $Re_\theta \approx 5.1 \times 10^4$ for a two-dimensional, canonical boundary layer experiencing a weak adverse pressure gradient ($\beta \approx 0.3$).

In figure 8(*a*,*b*), the momentum thickness at the reported stations in the experiments of Skare & Krogstad (1994) and Nagib *et al.* (2006) is compared with the prediction of the proposed model. It is noted that these experimental cases are, in fact, among the highest Reynolds number experiments for a canonical, two-dimensional, adverse pressure gradient turbulent boundary layer (see table 1 in Vila *et al.* (2020)). The provided power law distributions for the free stream velocity (U_e) in the experiments were used to determine the pressure gradient in the flow. In both these flows, the maximum error in the prediction of the momentum thickness is approximately 6 %. The power law distribution for the free stream velocity along the streamwise direction, according to (4.3), suggests that when $1/Re_\theta \ll 1$, the near linear growth of the momentum thickness is a valid solution to the differential equation, in agreement with experiments (Skare & Krogstad 1994). Similarly, the data of Perry (1966) as presented in Anderson (2011) shows a nearly linear growth of the boundary layer up to $Re_\theta \approx 0.97 \times 10^5$.

A non-equilibrium adverse pressure gradient flow from the recent experiments of Vila *et al.* (2020) is considered in figure 9. In contrast to the other two experiments, the free stream velocity does not follow a power law distribution along the streamwise direction, suggesting that the flow may experience history effects (Castillo & George 2001). Figure 9 suggests that the proposed model captures the growth of momentum thickness for this flow well. Appendix B also compares the predictions from the proposed model with the methods of Head and of Drela (see § 3) for this flow.

Appendix B. Performance of proposed model in comparison to Head's and Drela's integral methods for predicting momentum thickness

In this appendix, we compare the present method for predicting the momentum thickness of a turbulent boundary layer with the methods of Head (1958) and Drela & Giles (1987). A comparison between these methods and the proposed model is made on the flow over the Boeing speed bump, where the flow encounters both prolonged regions of favourable and adverse pressure gradients, and on the experimental boundary layer of Vila *et al.* (2020).

https://doi.org/10.1017/flo.2024.27 Published online by Cambridge University Press

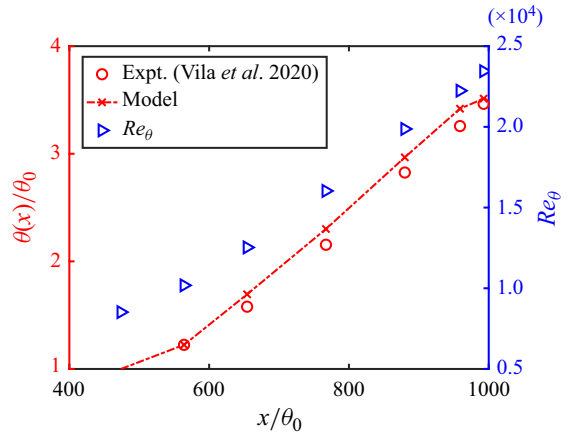

Figure 9. *The fit of θ/θ_0 for the experimental measurement stations reported in Vila et al. (2020) for a high Reynolds number ($8520 \leq Re_\theta \leq 23450$), non-equilibrium boundary layer ($0.38 \leq \beta \leq 2.19$). The left-hand and right-hand abscissas on these plots denote the prediction of θ and the true, experimental, value of Re_θ at the respective streamwise locations, respectively.*

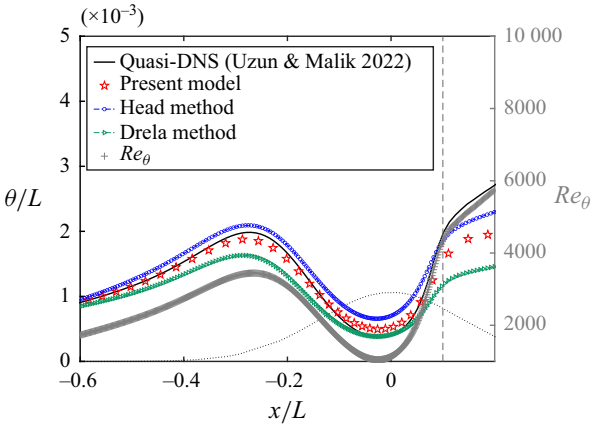

Figure 10. *A comparison between the proposed model, and existing methods of Head (1958) and Drela & Giles (1987) for the fit of θ/L versus the streamwise distance x/L for the flow over the Boeing speed bump studied by Uzun & Malik (2022). The vertical axis on the right-hand side of the figure presents the true, quasi-DNS Re_θ distribution as a function of x/L. The solid vertical line denotes the separation point obtained from the reference data. The bump geometry is shown with a black dashed line.*

For the Boeing speed bump flow in figure 10, all the methods perform reasonably in predicting the growth of momentum thickness initially ($x/L \leq -0.5$); followed by a slight under-prediction of θ from the approach of Drela & Giles (1987) in the favourable pressure gradient region (coincident with the decrease in Re_θ). The present method and the method of Head (1958) produce similar $\theta(x)$ distributions. For the higher Reynolds number boundary layer of Vila *et al.* (2020) in figure 11, all the methods perform well initially, but then the fits from the approaches of Head (1958) and Drela & Giles (1987) under-predict the momentum thickness, unlike the proposed method that still reasonably predicts θ as Re_θ reaches $O(10^4)$. These observations provide additional confidence in the improved performance offered by the proposed model over the existing methods of Head (1958) and Drela & Giles (1987).

https://doi.org/10.1017/flo.2024.27 Published online by Cambridge University Press

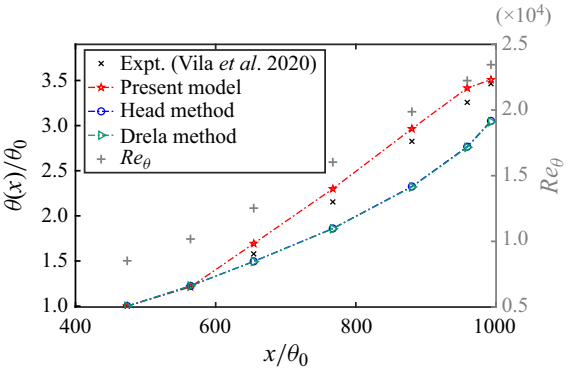

Figure 11. *A comparison between the proposed and the existing methods of Head (1958) and Drela & Giles (1987) for the fit of θ/θ_0 for the experimental measurement stations reported in Vila et al. (2020) at a Reynolds number ($8520 \leq Re_\theta \leq 23\,450$), adverse pressure gradient boundary layer ($0.38 \leq \beta \leq 2.19$). The vertical axis on the right-hand side of the figure presents the true, experimental, Re_θ distribution as a function of x/θ_0.*

References

Adair, D. 1987 Characteristics of a trailing flap flow with small separation. *Exp. Fluids* **5** (2), 114–128.

Alber, I. 1971 Similar solutions for a family of separated turbulent boundary layers. In *9th Aerospace Sciences Meeting*, p. 203.

Alber, I.E., Bacon, J.W., Masson, B.S. & Collins, D.J. 1973 An experimental investigation of turbulent transonic viscous-inviscid interactions. *AIAA J.* **11** (5), 620–627.

Anderson, C.M. 2011 Similarity in adverse pressure gradient turbulent flows. PhD thesis, Victoria University of Technology.

Bachalo, W.D.F. & Johnson, D.A. 1986 Transonic, turbulent boundary-layer separation generated on an axisymmetric flow model. *AIAA J.* **24** (3), 437–443.

Bobke, A., Vinuesa, R., Örlü, R. & Schlatter, P. 2017 History effects and near equilibrium in adverse-pressure-gradient turbulent boundary layers. *J. Fluid Mech.* **820**, 667–692.

Bourassa, C. & Thomas, F.O. 2009 An experimental investigation of a highly accelerated turbulent boundary layer. *J. Fluid Mech.* **634**, 359–404.

Castillo, L. & George, W.K. 2001 Similarity analysis for turbulent boundary layer with pressure gradient: outer flow. *AIAA J.* **39** (1), 41–47.

Castillo, L., Wang, X. & George, W.K. 2004 Separation criterion for turbulent boundary layers via similarity analysis. *J. Fluids Engng* **126** (3), 297–304.

Cebeci, T. & Bradshaw, P. 1977 *Momentum Transfer in Boundary Layers*. Hemisphere Publishing Corporation.

Cebeci, T., Mosinskis, G.J. & Smith, A.M.O. 1970 *Calculation of Viscous Drag and Turbulent Boundary Layer Separation on Two Dimensional and Axisymmetric Bodies in Incompressible Flows*. McDonnell Douglas Corporation.

Clauser, F.H. 1954 Turbulent boundary layers in adverse pressure gradients. *J. Aeronaut. Sci.* **21** (2), 91–108.

Clauser, F.H. 1956 The turbulent boundary layer. *Adv. Appl. Mech.* **4**, 1–51.

Coles, D.E. & Hirst, E.A. 1968 *Computation of Turbulent Boundary Layers–1968 AFOSR-IFP-Stanford Conference: Proceedings*, vol. 2. Thermosciences Division, Stanford University.

Curle, N. & Skan, S.W. 1957 Approximate methods for predicting separation properties of laminar boundary layers. *Aeronaut. Q.* **8** (3), 257–268.

Das, D.K. 1987 A numerical study of turbulent separated flows. In *Forum on Turbulent Flows–1987*, pp. 85–90. American Society of Mechanical Engineers.

Das, D.K., Naganathan, S., Kono, T. & Kulkarni, D. 2004 Comparison of three inner-variable approaches to establish an accurate method for turbulent boundary layers. *Naval Engrs J.* **116** (2), 85–102.

Das, D.K. & White, F.M. 1986 Integral skin friction prediction for turbulent separated flows. *J. Fluids Engng.* **108** (4), 476–482.

Devenport, W.J. & Lowe, K.T. 2022 Equilibrium and non-equilibrium turbulent boundary layers. *Prog. Aerosp. Sci.* **131**, 100807.

Dey, J. & Narasimha, R. 1990 An extension of the Thwaites method for calculation of incompressible laminar boundary layers. *J. Indian Inst. Sci.* **70** (1), 1–11.

Drela, M. 1989 XFOIL: an analysis and design system for low Reynolds number airfoils. In *Low Reynolds Number Aerodynamics: Proceedings of the Conference Notre Dame, Indiana, USA, 5–7 June 1989*, pp. 1–12. Springer.

Drela, M. & Giles, M.B. 1987 Viscous-inviscid analysis of transonic and low Reynolds number airfoils. *AIAA J.* **25** (10), 1347–1355.

https://doi.org/10.1017/flo.2024.27 Published online by Cambridge University Press

Eitel-Amor, G., Örlü, R. & Schlatter, P. 2014 Simulation and validation of a spatially evolving turbulent boundary layer up to $Re_\theta = 8300$. *Intl J. Heat Fluid Flow* **47**, 57–69.

Falkner, V.M. & Skan, S.W. 1931 LXXXV. Solutions of the boundary-layer equations. *Lond. Edinb. Dublin Phil. Mag. J. Sci.* **12** (80), 865–896.

Giles, M.B. & Drela, M. 1987 Two-dimensional transonic aerodynamic design method. *AIAA J.* **25** (9), 1199–1206.

Goc, K., Agrawal, R., Moin, P. & Bose, S. 2023 Studies of transonic aircraft flows and prediction of initial buffet onset using large-eddy simulations. In *AIAA Aviation 2023 Forum*.

Griffin, K.P., Fu, L. & Moin, P. 2021 General method for determining the boundary layer thickness in nonequilibrium flows. *Phys. Rev. Fluids* **6** (2), 024608.

Hancock, P.E. & Bradshaw, P. 1983 The effect of free-stream turbulence on turbulent boundary layers. *J. Fluids Engng* **105** (3), 284–289.

Head, M.R. 1958 Entrainment in the turbulent boundary layer. ARC R & M 3152.

Head, M.R. & Patel, V.C. 1968 Improved entrainment method for calculating turbulent boundary layer development. ARC R & M 3643.

Horton, H.P. 1968 Laminar separation bubbles in two and three dimensional incompressible flow. PhD thesis, Queen Mary University of London.

Kalkhoran, I.M. & Wilson, D.R. 1986 An integral method to investigate two-dimensional incompressible turbulent boundary layer. *Integral Methods in Science and Engineering*, pp. 221–226. Hemisphere Publishing Corporation.

Kline, S.J., Coles, D.E. & Hirst, E.A. 1969 *Computation of Turbulent Boundary Layers–1968 AFOSR-IFP-Stanford Conference: Proceedings*, vol. 1. Thermosciences Division, Stanford University.

Knopp, T., Reuther, N., Novara, M., Schanz, D., Schülein, E., Schröder, A. & Kähler, C.J. 2021 Experimental analysis of the log law at adverse pressure gradient. *J. Fluid Mech.* **918**, A17.

Ludwieg, H. & Tillmann, W. 1950 Investigations of the wall-shearing stress in turbulent boundary layers. *NACA Tech. Rep.* TM-1285.

Nagib, H.M., Christophorou, C. & Monkewitz, P.A. 2006 High Reynolds number turbulent boundary layers subjected to various pressure-gradient conditions. In *IUTAM Symposium on one Hundred Years of Boundary Layer Research*, pp. 383–394. Springer.

Nickels, T.B. 2004 Inner scaling for wall-bounded flows subject to large pressure gradients. *J. Fluid Mech.* **521**, 217–239.

Perry, A.E. 1966 Turbulent boundary layers in decreasing adverse pressure gradients. *J. Fluid Mech.* **26** (3), 481–506.

Simpson, R.L. 1981 A review of some phenomena in turbulent flow separation. *J. Fluids Engng* **103** (4), 520–533.

Simpson, R.L. 1983 A model for the backflow mean velocity profile. *AIAA J.* **21** (1), 142–143.

Skare, P.E. & Krogstad, P.-Å. 1994 A turbulent equilibrium boundary layer near separation. *J. Fluid Mech.* **272**, 319–348.

Sreenivasan, K.R. 1982 Laminarescent, relaminarizing and retransitional flows. *Acta Mech.* **44**, 1–48.

Stratford, B.S. 1959 The prediction of separation of the turbulent boundary layer. *J. Fluid Mech.* **5** (1), 1–16.

Swafford, T.W. 1983 Analytical approximation of two-dimensional separated turbulent boundary-layer velocity profiles. *AIAA J.* **21** (6), 923–926.

Talluru, K.M., Djenidi, L., Kamruzzaman, M. & Antonia, R.A. 2016 Self-preservation in a zero pressure gradient rough-wall turbulent boundary layer. *J. Fluid Mech.* **788**, 57–69.

Tanarro, Á., Vinuesa, R. & Schlatter, P. 2020 Effect of adverse pressure gradients on turbulent wing boundary layers. *J. Fluid Mech.* **883**, A8.

Thole, K.A. & Bogard, D.G. 1996 High freestream turbulence effects on turbulent boundary layers. *J. Fluids Engng* **118** (2), 276–284.

Thwaites, B. 1949 Approximate calculation of the laminar boundary layer. *Aeronaut. Q.* **1** (3), 245–280.

Uzun, A. & Malik, M.R. 2019 Wall-resolved large-eddy simulations of transonic shock-induced flow separation. *AIAA J.* **57** (5), 1955–1972.

Uzun, A. & Malik, M.R. 2022 High-fidelity simulation of turbulent flow past Gaussian bump. *AIAA J.* **60** (4), 2130–2149.

Vila, C.S., Vinuesa, R., Discetti, S., Ianiro, A., Schlatter, P. & Örlü, R. 2020 Experimental realisation of near-equilibrium adverse-pressure-gradient turbulent boundary layers. *Exp. Therm. Fluid Sci.* **112**, 109975.

Vinuesa, R., Negi, P.S., Atzori, M., Hanifi, A., Henningson, D.S. & Schlatter, P. 2018 Turbulent boundary layers around wing sections up to $Re_c = 1\,000\,000$. *Intl J. Heat Fluid Flow* **72**, 86–99.

Vinuesa, R., Örlü, R., Sanmiguel Vila, C., Ianiro, A., Discetti, S. & Schlatter, P. 2017 Revisiting history effects in adverse-pressure-gradient turbulent boundary layers. *Flow Turbul. Combust.* **99**, 565–587.

Volino, R.J. 1998 A new model for free-stream turbulence effects on boundary layers. *J. Turbomach* **120** (3), 613–620.

Weber, H.E. 1978 Boundary layer calculation for analysis and design. *J. Fluids Engng* **100**, 232–236.

White, F.M. 2008 *Fluid Mechanics*. McGraw Hill.

Williams, O., Samuell, M., Sarwas, E.S., Robbins, M. & Ferrante, A. 2020 Experimental study of a CFD validation test case for turbulent separated flows. In *AIAA Scitech 2020 Forum*, p. 0092.

Cite this article: Agrawal R, Bose S.T, Griffin K.P, Moin P (2024). An extension of Thwaites' method for turbulent boundary layers. *Flow*, *4*, E25. doi:10.1017/flo.2024.27